JBMR Plus, 2024, **8**, ziae031
https://doi.org/10.1093/jbmrpl/ziae031
Advance access publication: March 9, 2024
Research Article

Local application of zoledronate inhibits early bone resorption and promotes bone formation

Ming-Kai Hsieh[1,2], Chi-Yun Wang[2,3], Fu-Cheng Kao[1,2], Hui-Ting Su[1,2], Mei-Feng Chen[1,2], Tsung-Ting Tsai[1,2], Po-Liang Lai[1,2,*]

[1]Department of Orthopaedic Surgery, Spine Section, Chang Gung Memorial Hospital, Linkou, Taiwan and College of Medicine, Chang Gung University, Taoyuan 33305, Taiwan
[2]Bone and Joint Research Center, Chang Gung Memorial Hospital, Taoyuan 33305, Taiwan
[3]International Ph.D. Program in Innovative Technology of Biomedical Engineering and Medical Devices, Ming Chi University of Technology, Taishan Dist, New Taipei City 243303, Taiwan

*Corresponding author: Po-Liang Lai, Department of Orthopaedic Surgery, Chang Gung Memorial Hospital, No. 5, Fu-Shing St., Kweishan, Taoyuan 33305, Taiwan. (polianglai@gmail.com).

Abstract

Nonunion resulting from early bone resorption is common after bone transplantation surgery. In these patients, instability or osteoporosis causes hyperactive catabolism relative to anabolism, leading to graft resorption instead of fusion.
Systemic zoledronate administration inhibits osteoclastogenesis and is widely used to prevent osteoporosis; however, evidence on local zoledronate application is controversial due to osteoblast cytotoxicity, uncontrolled dosing regimens, and local release methods. We investigated the effects of zolendronate on osteoclastogenesis and osteogenesis and explored the corresponding signaling pathways. In vitro cytotoxicity and differentiation of MC3T3E1 cells, rat bone marrow stromal cells (BMSCs) and preosteoclasts (RAW264.7 cells) were evaluated with different zolendronate concentrations. In vivo bone regeneration ability was tested by transplanting different concentrations of zolendronate with β-tricalcium phosphate (TCP) bone substitute into rat femoral critical-sized bone defects. In vitro, zolendronate concentrations below 2.5×10^{-7} M did not compromise viability in the three cell lines and did not promote osteogenic differentiation in MC3T3E1 cells and BMSCs. In RAW264.7 cells, zoledronate inhibited extracellular regulated protein kinases and c-Jun n-terminal kinase signaling, downregulating c-Fos and NFATc1 expression, with reduced expression of fusion-related dendritic cell-specific transmembrane protein and osteoclast-specific Ctsk and tartrate-resistant acid phosphatase (. In vivo, histological staining revealed increased osteoid formation and neovascularization and reduced fibrotic tissue with 500 μM and 2000 μM zolendronate. More osteoclasts were found in the normal saline group after 6 weeks, and sequential osteoclast formation occurred after zoledronate treatment, indicating inhibition of bone resorption during early callus formation without inhibition of late-stage bone remodeling. In vivo, soaking β-TCP artificial bone with 500 μM or 2000 μM zoledronate is a promising approach for bone regeneration, with potential applications in bone transplantation.

Keywords: drug targeting, mesenchymal stem cells, bisphosphonate, osteoclast, pathway, rat femoral bone defect

Received: September 9, 2023. **Revised:** February 14, 2024. **Accepted:** March 3, 2024

Graphical Abstract

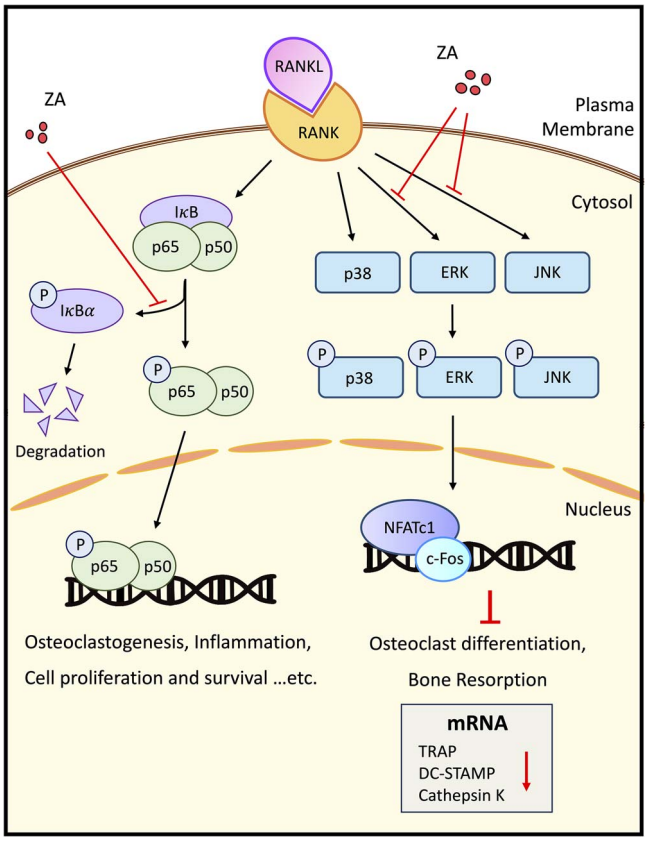

Introduction

The reconstruction of bone defects caused by fracture, infection, or tumor resection is a critical challenge for orthopedic and plastic surgeons. The three currently available treatment strategies for bone loss are based on autologous, allogeneic and synthetic biomaterial transplantation.[1-4] Regardless of the origin or structure of the implanted material, the bone graft is gradually revascularized and remodeled into new bone.[5] Neovascularization and resorption of new bone should be balanced to achieve graft remodeling and fusion. However, hyperactive catabolism rather than anabolism due to instability or osteoporosis leads to graft resorption instead of fusion in the clinic.[6,7] Since 1995, bisphosphonate, which is Food and Drug Administration approved, has been widely used as a skeletal antiresorptive agent to treat postmenopausal osteoporosis and is highly effective in limiting bone loss, preventing deterioration of the bone microarchitecture, and decreasing aging-related bone fracture risk.[6,8] Systemic administration of nitrogen-containing bisphosphonates, e.g., alendronate, ibandronate, and zoledronate, has been proven to inhibit osteoclastogenesis and is widely used to prevent osteoporosis. However, side effects such as erosive gastritis, acute phase reactions, hypoglycemia, osteonecrosis of the jaw bone, and atypical fracture limit the application of systemic administration.[7-10]

Local administration of bisphosphonates such as ibandronate and zolendronate (ZA) has been proven to be effective in reducing bone resorption in animal studies; however, some aspects, such as cytotoxicity to osteoblasts, local application using intravenous regimens and local released concentrations, are still unclear, making the results unreliable.[11-14]

The osteoblastogenic effect of ZA remains controversial.[11,15,16] Studies have shown that ZA has a positive influence on human bone marrow stromal cell (BMSC) differentiation into osteoblasts due to the overexpression of key bone-related genes, revealing the high biological potency of this drug; however, with a relatively low dose (10^{-8} M), effects of osteoblast induction medium cannot be excluded, and drugs with excipients, such as Zometa® (Novartis, Switzerland) and Aclasta® (Novartis, Switzerland), limit the real effect of ZA.[16-19] In contrast, in vitro studies showed that ZA at noncytotoxic levels inhibited angiogenesis and osteoblastogenesis in placental MSCs, and the osteogenic effect was observed at only very low concentrations.[13,15]

The purpose of this study was to identify a concentration of ZA that maximally inhibits osteoclastogenesis without interfering with osteoblastogenesis. The underlying pathway by which osteoclastogenesis is induced by ZA was also clarified. We investigated the ability of ZA-loaded tricalcium phosphate (TCP) scaffolds to inhibit excessive resorption and promote

bone formation through in vivo transplantation in the rat femoral condyle.

Materials and methods

In vitro *cellular response to different concentrations of ZA*

Cell culture of rat BMSCs, mouse MC3T3-E1 cells, and preosteoclasts (RAW264.7 cells)

The research proposal was approved by the Institutional Animal Care and Use Committee and adhered to the Guide for the Care and Use of Laboratory Animals (2020121505) in accordance with ARRIVE guidelines. Rat BMSCs were isolated from the femoral shafts of 4-week-old Sprague–Dawley male rats after flushing with 10 mL of culture medium (low-glucose Dulbecco's Modified Eagle Medium - DMEM; Gibco™, Invitrogen Corp., Carlsbad, CA) supplemented with 10% fetal bovine serum (FBS), 100 μg/mL penicillin and 100 U/mL streptomycin.[20] The released cells were collected in three 10-cm dishes containing 15 mL culture medium and incubated in a humidified atmosphere of 95% air with 5% CO_2 at 37°C. The nonadhered cells were removed after incubation for 3 days, and the culture medium was exchanged with fresh culture medium every 2 days. After the BMSCs reached approximately 80% confluence in 5 days, they were detached by incubation with phosphate-buffered saline (PBS; GIBCO™, Invitrogen Corp., Carlsbad, CA) containing 0.25% trypsin–EDTA (GIBCO™, Invitrogen Corp., Carlsbad, CA) at 37°C for 5 min and centrifugation at 1500 rpm for 5 min at 4°C. The cells were then gently suspended in 6 mL culture medium and used for further experiments.

The mouse preosteoblast cell line MC3T3-E1[21,22] was cultured in minimum essential medium-alpha (MEM-α) (Gibco) supplemented with 10% FBS (Gibco) and antibiotic solution (100 U/mL penicillin and 100 μg/mL streptomycin). The cells were maintained at 37°C in a humidified incubator supplied with 5% CO_2.

RAW264.7 mouse macrophages (osteoclast precursor, ATCC TIB-71, Manassas, VA, USA)[23] were seeded in 96-well tissue culture plates with DMEM (10% FBS, 1% penicillin–streptomycin, and 1.5 g/L sodium bicarbonate) at a density of 1.8×10^4 cells/cm^2 and incubated at 37°C under 5% CO_2 and 95% humidity overnight.

Cell viability

MC3T3-E1 cells and BMSCs were cultured on 96-well tissue culture plates at a cell density of 3×10^3 cells/cm^2 and treated with different concentrations of ZA (10^{-9}, 10^{-8}, 10^{-7}, 2.5×10^{-7}, 5×10^{-7}, and 10^{-6} M) (PHR1893, Sigma–Aldrich Corp., St. Louis, MO, USA) for 3 days. For BMSCs and MC3T3-E1 cells, osteoinduction medium (OIM), composed of complete MEM-α medium enriched with 10^{-7} M dexamethasone (Sigma–Aldrich Corp., St. Louis, MO, USA), 10 mM β-glycerophosphate (Sigma–Aldrich Corp., St. Louis, MO, USA) and 50 μg/mL ascorbic acid (Sigma–Aldrich Corp., St. Louis, MO, USA),[20,24] was added to the wells, and the cells were cultured for the indicated time in an incubator humidified with 95% air and 5% CO_2 at 37°C.

RAW264.7 cells were seeded at a density of 1.8×10^4 cells/cm^2 and cultured in DMEM supplemented with 10% FBS and 1% penicillin and streptomycin for 24 h. Osteoclast induction medium with 50 ng/mL receptor activator of nuclear factor- κ B ligand (RANKL, recombinant human soluble RANK ligand, 462-TR, R&D Systems, Minneapolis, USA) was added to the wells at the same time, followed by further incubation at 37°C for 1 to 6 days.[25]

On day 6, 100 μL of growth medium and 10 μL of Cell Counting Kit-8 (CCK-8, Dojindo, Rockville, MD, USA) solution were added to each well of the plate. The plate was then incubated for 1–4 hours at 37°C with 5% CO_2. Absorbance was measured at 450 nm using a microplate reader (BioTek Synergy HTX Multimode Reader, Santa Clara, CA, USA).

Osteogenesis evaluation

Alkaline phosphatase staining and activity

For staining, BMSCs and MC3T3-E1 cells in the wells were washed twice with PBS and fixed for 1 min using 60% (v/v) citrate solution comprising 0.6 mL citrate concentrate solution (Sigma) in 29.4 mL deionized water and 20 mL acetone. The wells were rinsed with deionized water and stained overnight with alkaline phosphatase staining solution. The alkaline phosphatase staining solution was a mixture of one part of naphthol AS-MX alkaline solution (Sigma) and 24 parts fast violet stain solution (Sigma). The next day, the staining solution was removed, and the wells were washed five times with deionized water. Images of the stained wells were captured with a digital camera (Canon, PowerShot SX50 SH). To measure the alkaline phosphatase activity with the enzyme-linked immunosorbent assay (ELISA), cells in each well were washed twice with PBS and lysed with radioimmunoprecipitation assay (RIPA) lysis buffer (Sigma–Aldrich Corp., St. Louis, MO, USA) mixed with a protease inhibitor cocktail (Sigma) to collect the total protein from each well. The alkaline phosphatase activity of each group was determined using an alkaline phosphatase assay kit (Abcam, Cambridge, MA, USA). All procedures were performed according to the manufacturer's guidelines, and absorbance was measured at a 405 nm wavelength using an ELISA reader (BioTek Synergy HTX Multimode Reader, Santa Clara, CA, USA).

Calcium deposition assay with Alizarin red S (ARS) staining and quantification

BMSCs and MC3T3-E1 cells in the wells were washed twice with PBS before being fixed with 4% paraformaldehyde in PBS at room temperature for 15 min. Subsequently, the solution was removed, and the wells were washed three times with ddH_2O. Then, 2% Alizarin red S (ARS) staining solution was applied and incubated at room temperature for 30 min. The staining agent was removed, and the wells were washed 3–5 times with ddH_2O. Images of the stained wells were captured with a digital camera (Canon, PowerShot SX50 SH). To quantify the results of ARS staining,[26] the dye was desorbed using 10 wt% cetylpyridinium chloride (Sigma, C9002) for 1 hour, and the absorbance was read at 620 nm using an ELISA reader (BioTek Synergy HTX Multimode Reader, Santa Clara, CA, USA).

Osteogenic differentiation and quantitative real-time polymerase chain reaction (RT–PCR)

BMSCs and MC3T3-E1 cells attached to the wells were dissociated with trypsin and collected for differentiation analysis. The total RNA was then extracted and reverse transcribed into cDNA using a PrimeScript™ RT Master Mix synthesis kit (RR036, Takara, Tokyo, Japan) following the manufacturer's instructions. The expression levels of

Table 1. Primer sequences for real time PCR analysis.

Gene	Primer Sequence (5' ➔ 3')
Mouse Ctsk Forward	CTCGGCGTTTAATTTGGGAGA
Mouse Ctsk Reverse	TCGAGAGGGAGGTATTCTGAGT
Mouse TRAP Forward	CACGAGAGTCCTGCTTGTC
Mouse TRAP Reverse	AGTTGGTGTGGGCATACTTC
Mouse OPN Forward	AGCAAGAAACTCTTCCAAGCAA
Mouse OPN Reverse	GTGAGATTCGTCAGATTCATCCG
Mouse OCN Forward	TGACAAAGCCTTCATGTCCAAG
Mouse OCN Reverse	CGTTTGTAGGCGGTCTTCAAG
Mouse ALP Forward	AACCCAGACACAAGCATTCCC
Mouse ALP Reverse	AATTCATACTGCATGTCCCCG
Mouse RUNX2 Forward	CAACAAGACCCTGCCCGT
Mouse RUNX2 Reverse	TCATAACAGCGGAGGCATTTC
Mouse NFATc1 Forward	CTCGAAAGACAGCACTGGAGCAT
Mouse NFATc1 Reverse	CGGCTGCCTTCCGTCTCATAG
Mouse c-Fos Forward	CCAGTCAAGAGCATCAGCAA
Mouse c-Fos Reverse	AAGTAGTGCAGCCCGGAGTA
Mouse DC-STAMP Forward	AAAACCCTTGGGCTGTTCTT
Mouse DC-STAMP Reverse	AATCATGGACGACTCCTTGG
Mouse 18S Forward	GACTCAACACGGGAAACCTC
Mouse 18S Reverse	AGACAAATCGCTCCACCAAC

Ctsk, Cathepsin K; TRAP, Tartrate Resistant Acid Phosphatase; OPN, Osteopontin; OCN, Osteocalcin; ALP, Alkaline Phosphatase; RUNX2, Runt-related transcription factor 2; NFATc1, Nuclear Factor of Activated T Cells 1; DC-STAMP, Dendritic Cell–Specific Transmembrane Protein.

the osteoblastic markers ALP, osteocalcin (OCN), and osteopontin (OPN) were quantified using SYBR Green Master mix (Applied Biosystems™, Waltham, Massachusetts, USA) and a QuantStudio 5 Real-Time PCR System (Applied Biosystems™, Waltham, Massachusetts, USA). Forward and reverse primers were designed with Primer Express Software (Applied Biosystems). The sequences of the forward and reverse primers used in the study are shown in Table 1. The expression of 18S rRNA was examined as the endogenous control. Relative transcript levels were calculated from the relative standard curve constructed from stock cDNA dilutions and divided by the target quantity of the control following the manufacturer's instructions.

Osteoclastogenesis evaluation

RAW264.7 cells were seeded in 96-well tissue culture plates at a density of 1.8×10^4 cells/cm^2 and cultured in DMEM supplemented with 10% FBS and 1% penicillin and streptomycin for 24 h. Then, the cell culture was supplemented with 50 ng/mL RANKL and various concentrations of ZA (10^{-9}, 10^{-8}, 10^{-7}, 2.5×10^{-7}, 5×10^{-7}, and 10^{-6} M) for 3 days at 37°C, and the cell culture medium was replaced with fresh complete medium every 2–3 days until many mature osteoclasts formed. To evaluate osteoclast differentiation at the end of each incubation, the cells were washed twice and fixed with fixation solution for 5 min.

Tartrate-resistant acid phosphatase staining

The tartrate-resistant acid phosphatase (TRAP) staining kit (MK300, Takara, Tokyo, Japan) was then used to stain for TRAP, an osteoclast marker, according to the manufacturer's instructions.[27] After culturing, stained TRAP-positive multinucleated cells with >3 nuclei were identified under an inverted microscope (C13220-01, NanoZoomer S360 Digital slide scanner, Hamamatsu, Shizuoka, Japan) and considered osteoclast-like cells. We analyzed and compared the number of TRAP-positive cells among all concentrations using an NDP.View2 Analyzer (Hamamatsu, Shizuoka, Japan). Three images were captured per well. These images were analyzed using ImageJ software.

Bone resorption assay

The osteoclast bone resorption assay was performed using a commercially available bone resorption assay kit[28,29] (CosMo Bio, Tokyo, Japan). The cells were treated with various concentrations of ZA (10^{-9}, 10^{-8}, 10^{-7}, 2.5×10^{-7}, 5×10^{-7}, and 10^{-6} M) and RANKL (50 ng/mL) and incubated on fluoresceinamine-labeled chondroitin sulfate-bound calcium phosphate-coated microplates for 5 days. The mature osteoclasts on the microplates were then washed out using 5% sodium hypochlorite, and resorption pits were visualized under a scanning electron microscope (IX71, Olympus, Tokyo, Japan). The total number and area of resorption pits were quantified and compared using ImageJ software (1.53 k).

Osteoclastogenesis and quantitative real-time polymerase chain reaction (RT–PCR)

RAW264.7 cells were seeded onto 96-well plates at a density of 1.8×10^4 cells/cm^2 and cultured in complete medium with ZA at 37°C for 0, 1, 3 and 5 days with 50 ng/mL RANKL. Total RNA was then extracted and reverse transcribed into cDNA using a cDNA synthesis kit (TaKaRa, Japan) following the manufacturer's instructions. The expression levels of the osteoclastic markers TRAP, cathepsin K (Ctsk), OPN, c-fos, DC-STAMP, and NFATC-1[30-32] were quantified using SYBR Green Master mix (TaKaRa, Japan) and a Step One Plus RT–PCR instrument (ABI7500, USA). Forward and reverse primers were designed with Primer Express Software (Applied Biosystems). The sequences of the forward and reverse primers used in this study are shown in Table 1. The expression of GAPDH was examined as the endogenous control. Relative transcript levels were calculated from the relative standard curve constructed from stock cDNA dilutions and divided by the target quantity of the control following the manufacturer's instructions.

Assays of osteoclastogenesis-related pathways

The RAW264.7 cell samples lysed in RIPA buffer with Protease Inhibitor Cocktail (P8340, Sigma–Aldrich) and Phosphatase Inhibitor Cocktail 2 and 3 (P5726 and P0044, Sigma–Aldrich) were boiled in a sodium dodecyl sulfate (SDS) sample buffer containing 0.5 M β-mercaptoethanol. The samples were separated on 10% SDS-polyacrylamide gels and transferred to polyvinylidene fluoride membranes (Millipore, MA, USA). The membranes were blocked with 5% skim milk in Tris–HCl-buffered saline with Tween® 20 (TBST) for 1 hour at room temperature. The antibodies used were from Cell Signaling Technology (MA, USA). Membranes were incubated with anti-p38 (1:5000)/phosphorylated p38 antibody (1:1000), anti-ERK (extracellular signal-regulated kinase) (1:20000)/phosphorylated ERK antibody (1:10000), anti-JNK (c-Jun N-terminal kinase) (1:5000)/phosphorylated JNK antibody (1:2000), anti-p65 (1:1000)/phosphorylated p65 antibody (1:2000), anti-IκBα(1:1000)/phosphorylated IκBα antibody (1:1000), and GAPDH antibody (1:10000) at 4°C overnight.[33,34] The membranes were then washed three times with TBST buffer. The Western blots were incubated with secondary antibodies (1:2000) (anti-rabbit IgG HRP, GENA934, Cytiva, USA; anti-mouse IgG HRP, NEF822001, PerkinElmer, Akron, Ohio, USA) at room temperature for 1 hour and developed using Western Lightning Plus-ECL (PerkinElmer, Akron, Ohio, USA) for visualization on X-ray film.

In vivo *experimental design*

This study included a total of 24 male skeletally healthy Sprague–Dawley rats (250–300 g, 12 weeks old) housed in a light- and temperature-controlled environment. The study was carried out in strict accordance with the recommendations in the *Guide for the Care and Use of Laboratory Animals* of the National Institutes of Health. All animals were used under animal protocols approved by the Institutional Animal Care and Use Committee of Chang Gung Memorial Hospital (2020121505) and housed accordingly. β-Tricalcium phosphate (β-TCP) columns (diameter: 4 mm, length: 4 mm, porosity: 70%; HOYA (Tokyo, Japan)) were used as the scaffold in this study. To prepare the materials for the ZA groups, 250 μL of 50, 500, or 2000 μM ZA (Sigma–Aldrich Corp., St. Louis, MO, USA)[14] and 250 μL of normal saline for the control group was loaded onto each piece of β-TCP column and soaked for 1 hour until all liquid was absorbed.

The four treatment groups included implantation of β-TCP columns with normal saline (NS, n = 6), implantation of scaffolds and 50 μM ZA (50 μM; n = 6), implantation of scaffolds and 500 μM ZA (500 μM; n = 6) and implantation of scaffolds and 2000 μM ZA (2000 μM; n = 6). The treatments were determined for each animal with a randomization chart. These doses fall within a range where previous studies have demonstrated a clinically significant treatment effect through local administration.[35,36]

Surgical procedure

All experimental procedures were performed under a standard anesthetic/analgesic protocol as described in previous studies.[37,38] An incision of 20 mm in length was created above the knee joint in the dorsal femoral region of each animal. To establish the femoral condyle defect model, a cylindrical bone defect with a diameter of 4 mm and a depth of 4 mm was generated using a trephine bur (ACE Surgical Supply Co., Inc., USA). To avoid thermal bone injury, continuous saline irrigation was carried out during burring. After implantation of scaffolds, the periosteum and skin were stitched with 4–0 nylon sutures. An intramuscular dose of ketoprofen (25 mg/mL) and a subcutaneous dose of cefazolin sodium (100 mg/mL) were given to all animals postsurgically. The wound condition, diet, activity and signs of infection were monitored in the animals daily.

Euthanization and preparation of specimens

Five animals in each group were euthanized 6 and 12 weeks after surgery. The rats were euthanized via carbon dioxide asphyxiation, and the retrieved specimens after en bloc excision were fixed in 10% neutral formalin for further evaluation.

Image analysis

X-ray imaging and microcomputed tomography (μCT) were performed in the 6th and 12th weeks after implantation. Block samples, including the surgical sites, were harvested and preserved in 4% paraformaldehyde at 37°C for 48 h. The samples collected at 6 and 12 weeks from each group were scanned using a μCT system (Explore Locus; GE Healthcare, Chalfont St. Giles, Buckinghamshire, UK) in high-resolution scanning mode.

Histological analysis

The implanted tissue blocks were decalcified in 10% EDTA for 3 weeks at room temperature, dehydrated using an increasing alcohol gradient, serially cut into 5-μm-thick slices, immersed in paraffin, and mounted on glass slides. Longitudinal sections were stained with hematoxylin–eosin and Masson's trichrome for bone and cartilage and TRAP for osteoclasts and imaged under an optical microscope (DXM200F Digital Camera; Nikon, Tokyo, Japan). The volume of regenerated bone within the defects was calculated from images of Masson's trichrome staining by using MicroVIEW software (GE Healthcare).

Statistical analyses

The in vitro experiments were performed three times and results are presented as the means ± standard deviations. The statistical analyses were conducted by using Microsoft office Excel 2019 (Microsoft Corporation, State of Washington, USA). Comparisons among multiple groups were performed using one-way analysis of variance. Differences were considered statistically significant when the P value < 0.05.

Results

Cytotoxic effects of ZA on BMSCs, MC3T3E-1 cells and RAW264.7 cells

The viability of BMSC, MC3T3E-1, and RAW264.7 cells was compared by performing a Cell Counting Kit-8 (CCK-8) assay on cells cultured in induction medium containing different concentrations of ZA (10^{-9}, 10^{-8}, 10^{-7}, 2.5×10^{-7}, 5×10^{-7}, and 10^{-6} M) for 3 days. The cytotoxicity of various cell lines exposed to different concentrations of ZA is assessed using CCK-8. The cell viability rate is determined by comparing the outcomes to those of the untreated control group. The results showed that increasing the ZA concentration to

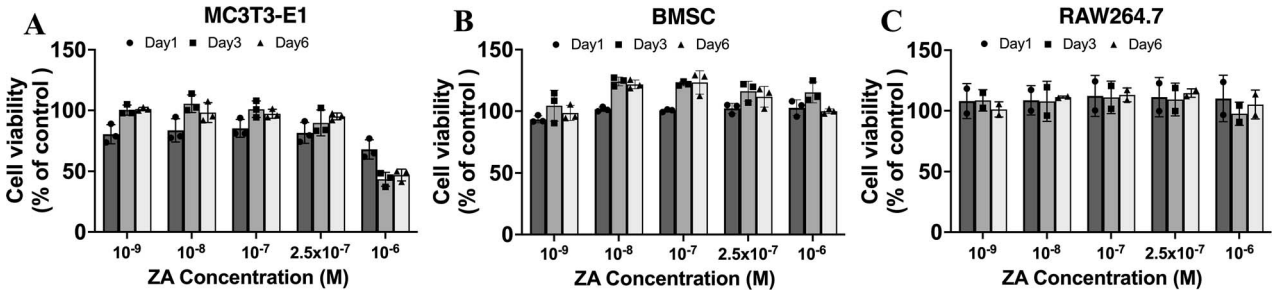

Figure 1. The cytotoxic effects of ZA on MC3T3E-1 cells (A), BMSCs (B), and RAW264.7 cells (C).The results showed that increasing the ZA concentration to 2.5×10^{-7} M did not compromise the viability of the three cell types.

2.5×10^{-7} M did not compromise the viability of the three cell types (Figure 1).

Effect of ZA on the osteogenic differentiation of MC3T3E-1 cells and BMSCs

Figure 2A and B shows the quantification of ALP activity, an early marker of bone formation.[22] In both BMSCs and MC3T3E-1 cells, ALP levels significantly increased in all groups on day 14 compared to those on day 7, indicating that ZA had no inhibitory effect on early osteogenesis. ARS staining, a late marker of bone formation, was used to assess bone mineralization in cells treated with various concentrations of ZA (Figure 2C-F). On day 28, all groups with ZA concentrations below 2.5×10^{-7} M showed positive staining with a deep red color, indicating bone nodule formation. The ARS quantification assay demonstrated similar values for ZA concentrations below 2.5×10^{-7} M and OIM groups in both cell lines. However, when comparing ZA concentrations below 2.5×10^{-7} M and OIM groups, ZA concentrations of 10^{-6} M showed significant lower values on day 21 and day 28 in M3T3E-1 cells and on day 21 in BMSCs ($P < 0.05$).

To assess the osteoblastic effect of ZA on the preosteoblastic cell line M3T3E-1, we evaluated the expression of the osteoblast-specific genes ALP, OCN, and OPN (Figure 3) after 7, 14, and 21 days of exposure to control medium, OIM, and ZA (at concentrations of 10^{-9}, 10^{-8}, 10^{-7}, and 2.5×10^{-7} M).[15] The results demonstrated that the expression of ALP was upregulated in cells cultured in OIM alone or supplemented with ZA in the first two weeks, but there is no significance between ZA treated groups and OIM groups. In the OCN expression, concentrations of ZA at 10^{-9}, 10^{-7}, and 2.5×10^{-7} M exhibited significantly higher values than OIM on day 7. Similarly, within the OPN group, ZA at concentrations of 10^{-7} and 2.5×10^{-7} M showed significantly higher values compared to OIM on day 7 ($^{*}P < 0.05$). The variable increase in the expression of OCN and OPN, in comparison to the OIM groups, did not provide support for ZA having a positive effect on bone formation. No significant differences in levels were observed between OIM and ZA groups at other time points.

ZA suppresses RANKL-induced osteoclastic differentiation and bone resorption in RAW264.7 cells

We assessed the inhibitory effect of ZA on RANKL-induced osteoclastogenesis by measuring TRAP staining of RAW264.7 cells incubated with different concentrations of ZA (10^{-9}, 10^{-8}, 10^{-7}, and 2.5×10^{-7}, 10^{-6} M) in the presence of 50 ng/mL RANKL (Figure 4). Large multinucleated TRAP-positive osteoclast cells were observed in ZA-treated groups at day 5 in the presence of RANKL. When compared to RANKL-only groups, the number of osteoclasts was significantly suppressed by ZA at various time points on day 3, day 5, and day7 (Figure 4B). We conducted a resorption pit assay to investigate the effects of various concentrations of ZA (10^{-9}, 10^{-8}, 10^{-7}, and 2.5×10^{-7}, 10^{-6} M) on mature osteoclast activity (Figure 4C). The results showed a significant decrease in the area of osteoclast bone resorption pits in the ZA groups compared to the RANKL-only group (Figure 4D). The findings of the resorption pit assay were consistent with the TRAP staining and quantification data.

Furthermore, pretreatment with ZA strongly inhibited the RANKL-induced formation of TRAP-positive multinucleated osteoclasts and bone resorption pits. These results convincingly demonstrated that ZA inhibits the fusion of preosteoclasts and the bone resorption of mature osteoclasts.

Effects of ZA on the mRNA expression of osteoclast differentiation-specific genes in RAW264.7 cells

To further investigate the inhibitory effects of ZA on osteoclast formation, we conducted RT–qPCR analysis to evaluate the expression of specific osteoclastogenesis-related genes. Our results showed an increase in the expression of osteoclastic markers, including Ctsk, NFATc1, TRAP, DC-STAMP, and c-Fos, in RAW264.7 cells treated with RANKL alone (Figure 5). However, when treated with ZA for 3 days, the upregulation effect on osteoclast-specific gene expression was significantly suppressed, and downregulated expression of most osteoclast-specific mRNAs was observed in the presence of ZA (* $P < 0.05$ and ** $P < 0.01$, ZA treated groups compared to RANKL-only groups). These findings suggest that ZA inhibits the formation of osteoclasts by regulating the expression of osteoclastogenesis-specific genes.

ZA inhibits RANKL-induced p38 and JNK phosphorylation and inhibits downstream expression of NFATC1, DC-STAMP and c-Fos

To investigate the mechanisms by which ZA regulates osteoclastogenesis, we examined the protein levels of components of RANKL-induced signaling pathways using Western blot analysis. The mitogen-activated protein kinase (MAPK) family plays a key role in committing cells to the osteoclastic lineage and regulates downstream coregulators such as ERK, JNK, and p38 in the transcriptional regulation of target genes.[39-41] Our results showed that ZA significantly inhibited the phosphorylation of the ERK and JNK proteins within 5-15 minutes (* $p < 0.05$ and ** $P < 0.01$, ZA treated groups

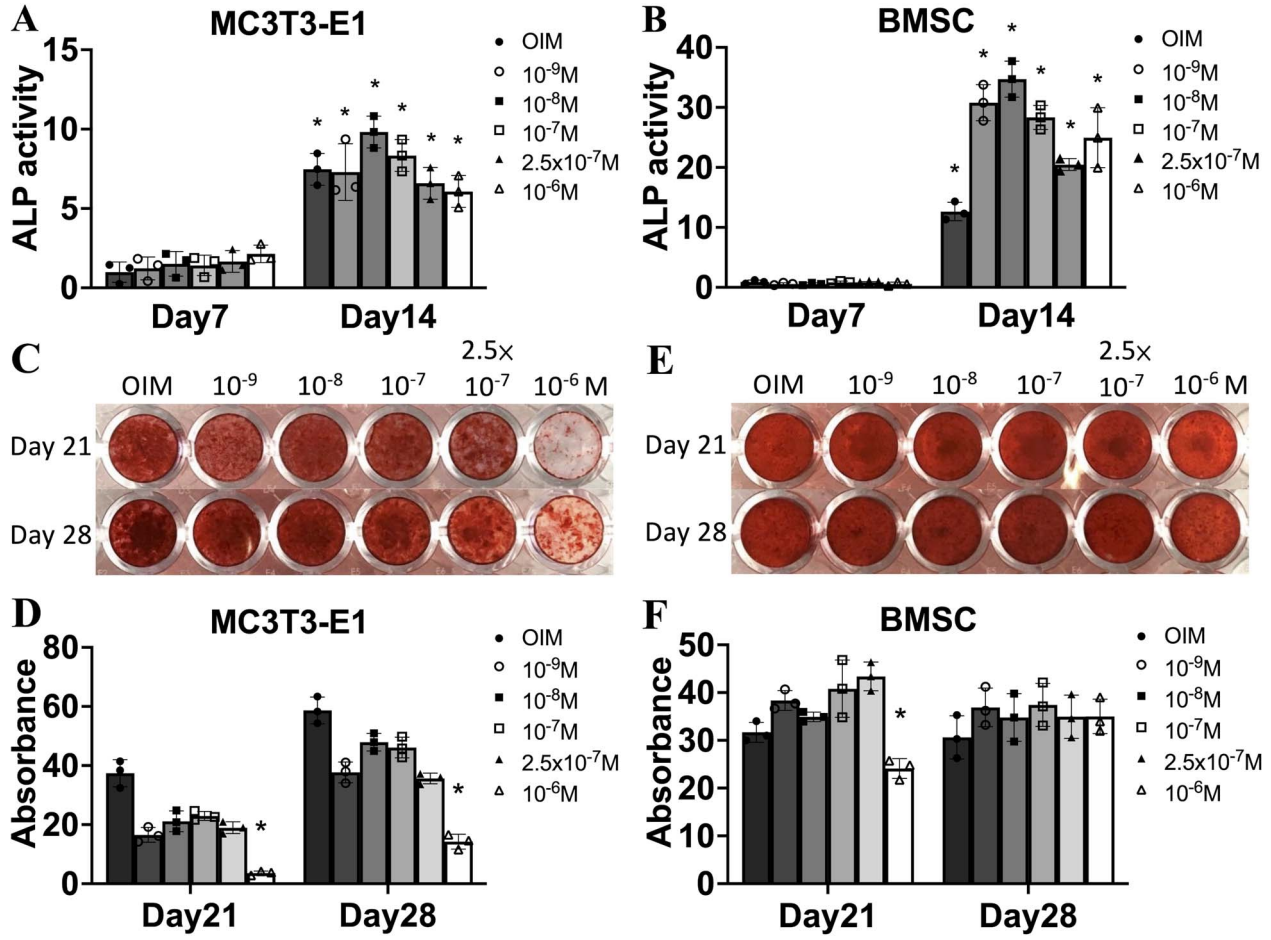

Figure 2. ALP levels significantly increased in the OIM- and ZA-treated groups in both BMSCs and MC3T3E-1 cells after the first two weeks (*$P < 0.05$) (a, B). On day 28, all groups with ZA concentrations below 2.5×10^{-7} M showed positive ARS staining with a deep red color, indicating bone nodule formation (C AND E). The ARS quantification assay demonstrated similar values for ZA concentrations below 2.5×10^{-7} M in both cell lines and no significant positive staining for ZA concentrations over 2.5×10^{-7} M in both cell lines from the 21st day to the 28st day ($P < 0.05$) (D and F). There is a lack of apparent statistical significance between the OIM and ZA added groups at each time point in the two cell types.

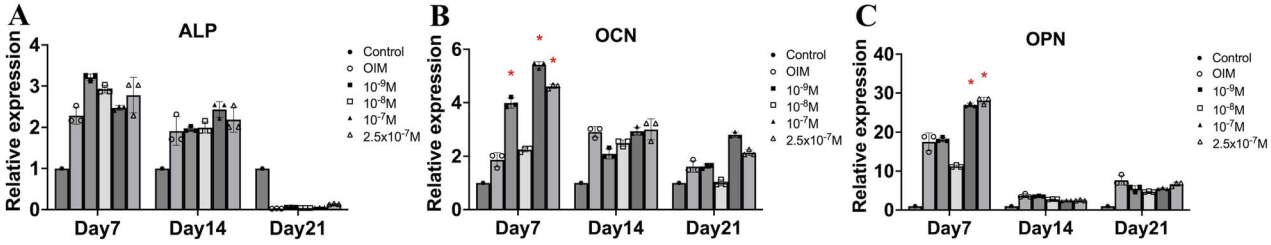

Figure 3. Osteogenesis differentiations of MC3T3E-1 cells for 7, 14, and 21 days of exposure to control medium, OIM, and ZA (at concentrations of 10^{-9}, 10^{-8}, 10^{-7}, and 2.5×10^{-7} M) were collected for quantitative RT-PCR. The expression levels of osteoblastic markers, ALP (A), was up-regulated in cells cultured in OIM alone or supplemented with ZA in the first 2 weeks. The expression of OCN (B) and OPN(C) was up-regulated until the third week. In the OCN expression, concentrations of ZA at 10^{-9}, 10^{-7}, and 2.5×10^{-7} M exhibited significantly higher values than OIM on day 7. Similarly, within the OPN group, ZA at concentrations of 10^{-7} and 2.5×10^{-7} M showed significantly higher values compared to OIM on day 7 (*$P < 0.05$). No significant differences in levels were observed between OIM and ZA groups at other time points.

compared to RANKL-only groups) but had no significant effect on the phosphorylation of p38 proteins (Figure 6A-C). These findings suggest that ZA inhibits ERK and JNK signaling by reducing the levels of p-ERK and p-JNK, leading to a reduction in osteoclast formation via suppression of RANKL-induced activation of these pathways. In Figure 6D, the rapid activation of the phosphorylation of IκBα, the inhibitor of NF-κB, was observed at 5 min following RANKL exposure (* $P < 0.05$, ZA treated groups compared to RANKL-only groups). Our study showed that ZA significantly inhibited the phosphorylation of IκBα proteins within 5-10 minutes but had no significant effect on the phosphorylation of p65 proteins which implied activation of NF-κB maybe not only through phosphorylation of IκBα.

In vivo *bone regeneration in rat femoral critical-sized defects*

In vivo *radiographic and micro-CT results*

All animals survived the study period without any complications. The osteogenic potential of the femoral defects was evaluated after 6 and 12 weeks. X-rays and micro-CTs in

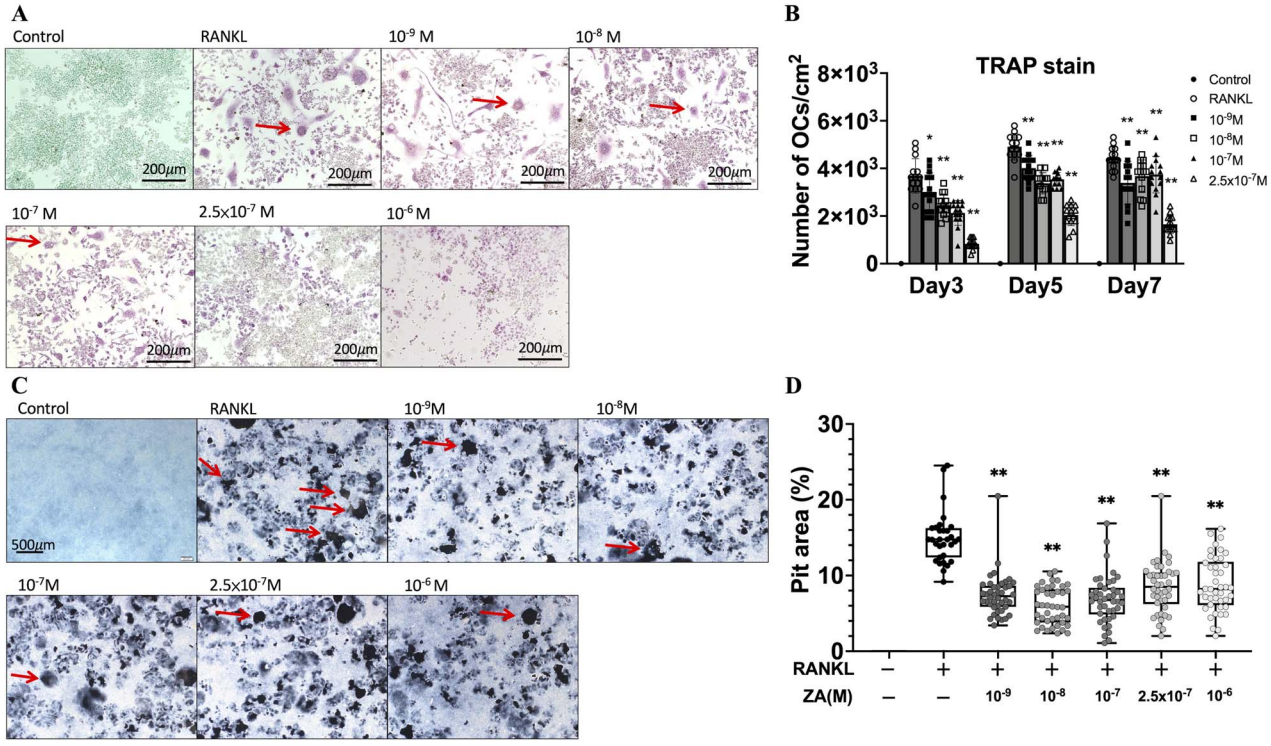

Figure 4. On day 7, the TRAP staining of RAW264.7 cells incubated with different concentrations of ZA showed that large multinucleated TRAP-positive osteoclast cells were observed in the presence of RANKL (A, red arrows) but the number decreased with the increasing concentration of ZA (* $P < 0.05$, ** $P < 0.01$) (B). A resorption pit assay was used to investigate the effect of various concentrations of ZA on mature osteoclast activity (C, red arrows). The results showed a significant decrease of pit areas in the ZA groups compared to the RANKL-only group (** $P < 0.01$) (D).

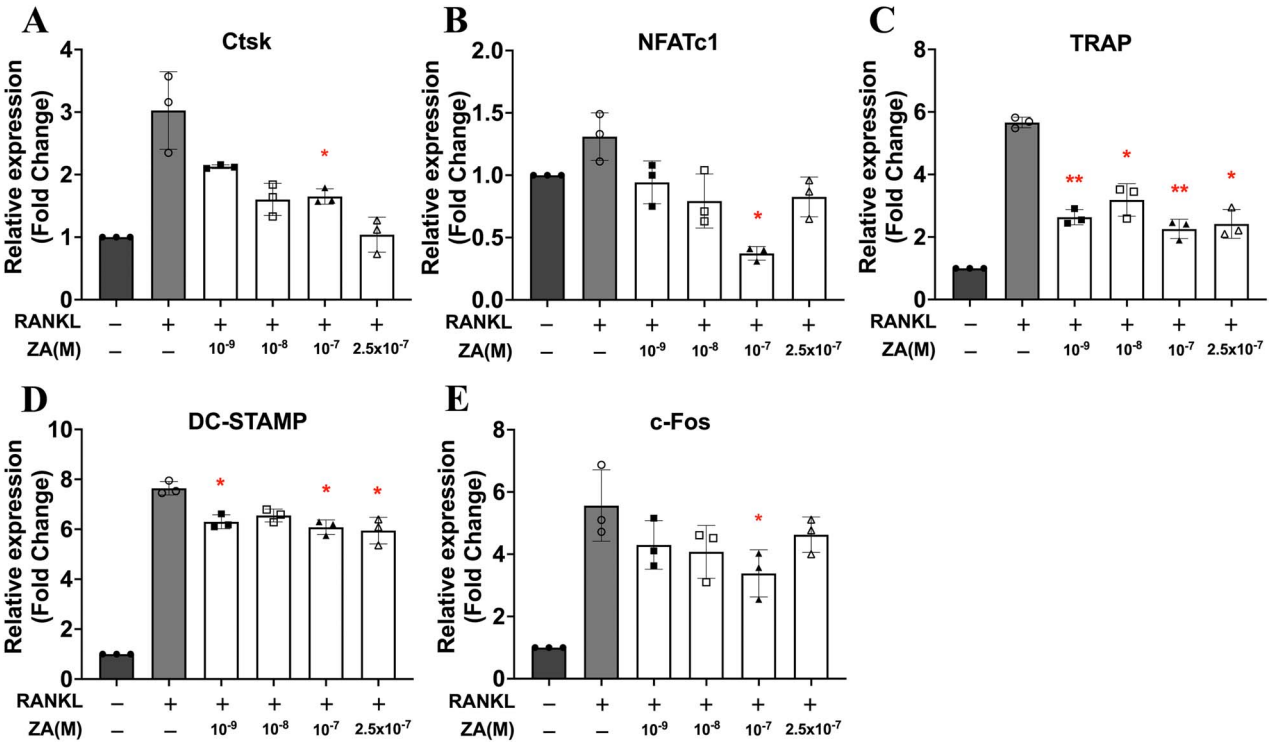

Figure 5. Expression of osteoclastogenesis-related genes of RAW264.7 cells treated with RANKL and various concentrations of ZA for 3 days were collected for RT-qPCR. The expression levels Ctsk(A), NFATc1(B), TRAP(C), DC-STAMP(D), and c-Fos(E) were up-regulated by RANKL-only and significantly down-regulated in the presence of ZA (* $P < 0.05$ and ** $P < 0.01$, ZA treated groups compared to RANKL-only groups).

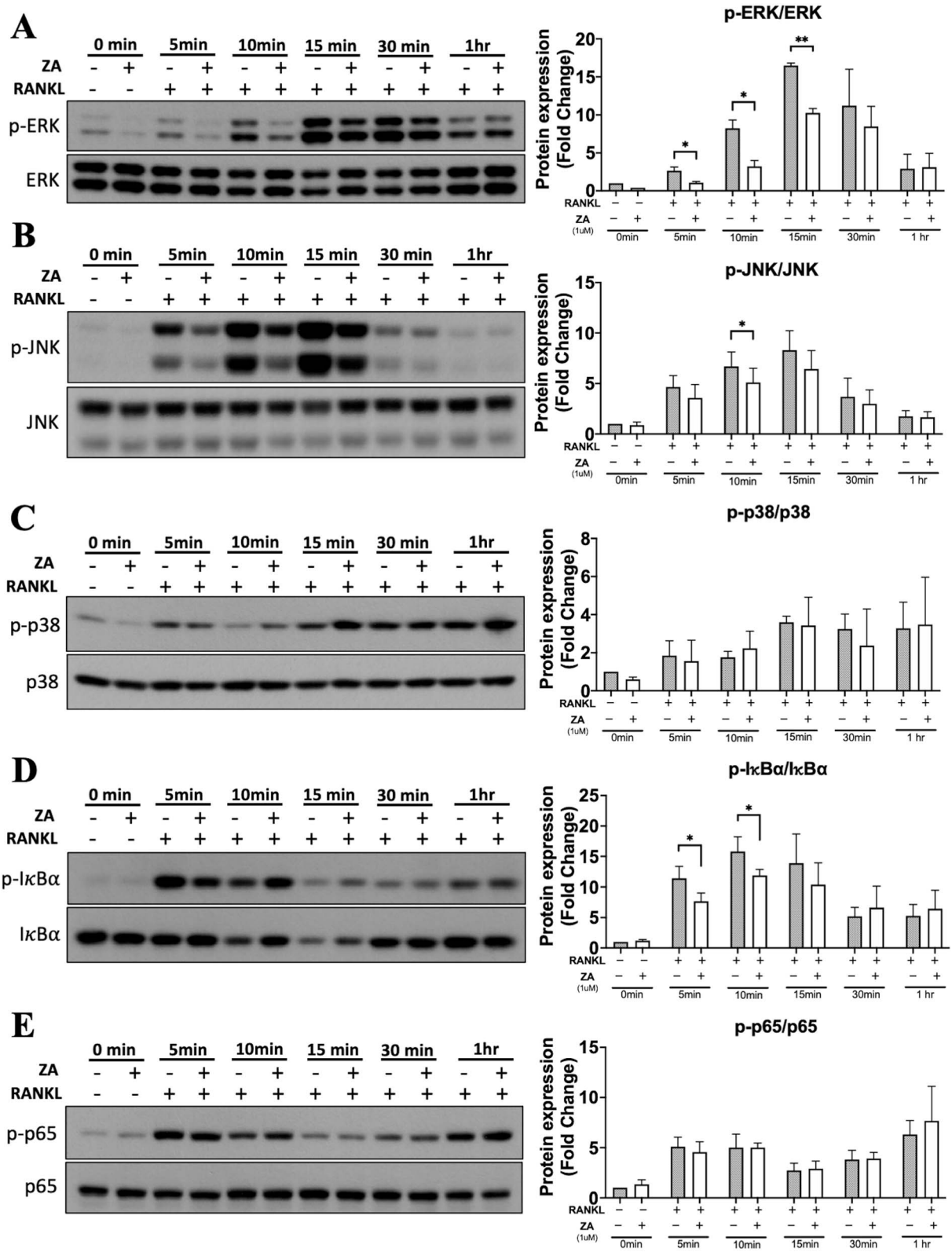

Figure 6. Signaling pathways of RAW264.7 cells treated with RANKL following pretreatment with ZA (1 μM) for 4 hrs. Western blot and band intensity ratios of (A) p-ERK/ERK, (B) p-JNK/JNK, (C) p-p38/9-38, (D) p-IκBα/IκBα, and (E) p-p65/p65 showed that ZA significantly inhibited the phosphorylation of ERK and JNK proteins within 5–15 min, but had no significant effect on the phosphorylation of p38 proteins(C). The rapid activation of the phosphorylation of IκBα was observed at 5 min following RANKL exposure showed that ZA significantly inhibited the phosphorylation of IκBα proteins within 5–10 min but had no significant effect on the phosphorylation of p65 proteins (* $P < 0.05$ and ** $P < 0.01$).

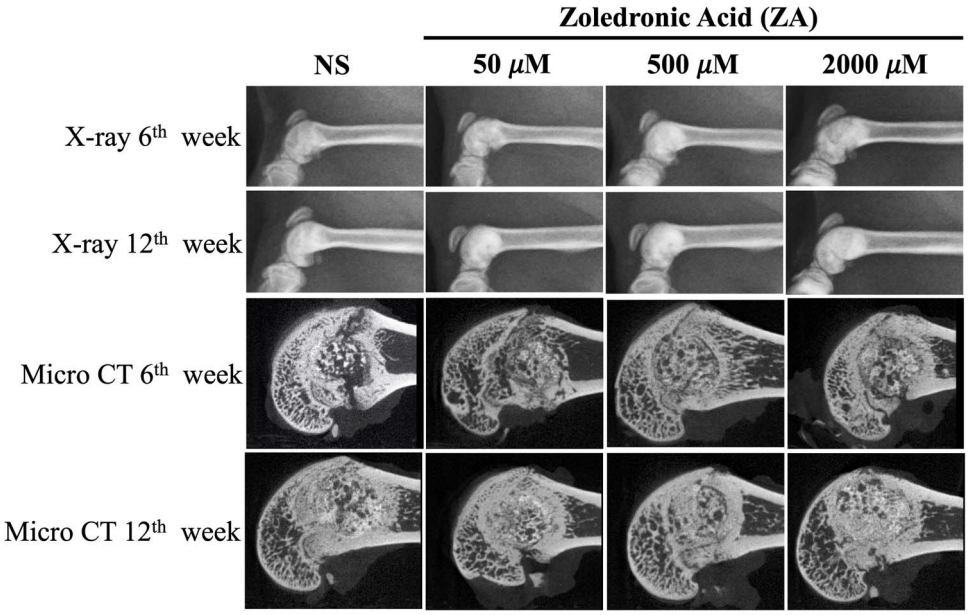

Figure 7. X-ray and micro-CT images of all groups. Increasing radiopacity was observed in all groups on X-rays from 6th week to 12th week. In the micro-CT scans at the sixth week, less surrounding bone resorption was observed in the 500 μM and 2000 μM groups compared to the NS and 50 μM groups. At the 12th week, lesser central bone resorption was detected in the 500 μM and 2000 μM groups, illustrated by more radiopacity at the center of the graft.

high-resolution mode were performed on five samples from each group (Figure 7). Increasing radiopacity was observed in X-rays from all groups from the 6th week to the 12th week. In the micro-CT scans from the sixth week, less surrounding bone resorption was observed in the 500 μM and 2000 μM groups than in the NS and 50 μM groups. Adequate bone formation with surrounding callus formation was observed in all groups. In the 12th week, less central bone resorption was detected in the 500 μM and 2000 μM groups.

Histologic analysis

Hematoxylin & eosin staining and Masson's trichrome staining were examined at various magnifications using a light microscope (Figure 8). In the sixth week, significant bone resorption was observed after H&E staining, and the implanted artificial bone was still visible in the 2000 μM group (Figure 8A, yellow arrow). More deposition of osteoids surrounding the contact surface of scaffolds was observed in the 500 μM and 2000 μM groups, but less was observed in the NS group (Figure 8A, yellow arrowhead). Masson's trichrome staining revealed thick, dense bone-like tissue surrounding the implanted β-TCP scaffolds in the ZA-treated groups, whereas this space was occupied by dense fibrous connective tissue with thin bone-like tissue in the NS groups (Figure 8B, yellow arrowhead). Neovascularization was evident inside the dense bone-like tissue (Figure 8B, yellow arrow) in the 500 μM and 2000 μM groups.

Histomorphometric analysis

The amount of new bone formation was quantified using Masson's trichrome-stained sections at 12 weeks postoperatively. Histomorphometric analysis showed that the ZA-treated groups exhibited more bone formation than the normal saline group: $68.99 \pm 9.18\%$ in the 2000 μM group, $63.80 \pm 10.27\%$ in the 500 μM group, $66.37 \pm 14.78\%$ in the 50 μM group and $45.81 \pm 14.63\%$ in the NS group (Figure 8C). Quantification of the mineralized tissue area revealed a significantly higher value for the 2000 μM group than for the normal saline group ($^{*}\ P < 0.05$).

Immunohistochemistry with TRAP staining

In the sixth week, more TRAP-positive osteoclast cells were observed in the NS groups, and almost no cells with positive staining were present in the 500 μM and 2000 μM groups (Figure 9A, red arrow). Quantification of the TRAP-staining revealed a significantly higher value for the normal saline groups than the ZA-treated groups ($^{*}\ P < 0.05$, $^{**}\ P < 0.01$, ZA-treated groups compared to normal saline groups). More osteoclasts were found in the ZA-treated groups in the 12th week than in the 6th week, indicating that local application did not interfere with osteoclast formation from new bone, which indicates that long-term bone remodeling was not inhibited (Figure 9B, red arrow). Quantification of the TRAP-staining showed a significantly higher value for the 500 μM and 2000 μM groups than the normal saline groups ($^{*}P < 0.05$, ZA-treated groups compared to normal saline groups).

Discussion

Studies conducted on animals have demonstrated that local administration of bisphosphonates such as ibandronate and zolendronate can decrease bone resorption, but cytotoxicity to osteoblast-related cells, the involved pathways, local applications using intravenous regimens, and local released concentrations are still poorly understood, rendering the results unreliable.[11,12,15,42] The objective of this study was to determine the optimal concentration of ZA for local administration to prevent osteoclastogenesis and activation of its underlying pathway while avoiding any interference with osteogenesis. In our in vitro study, we evaluated the viability of MC3T3-E1 cells, BMSCs, and RAW264.7 cells treated

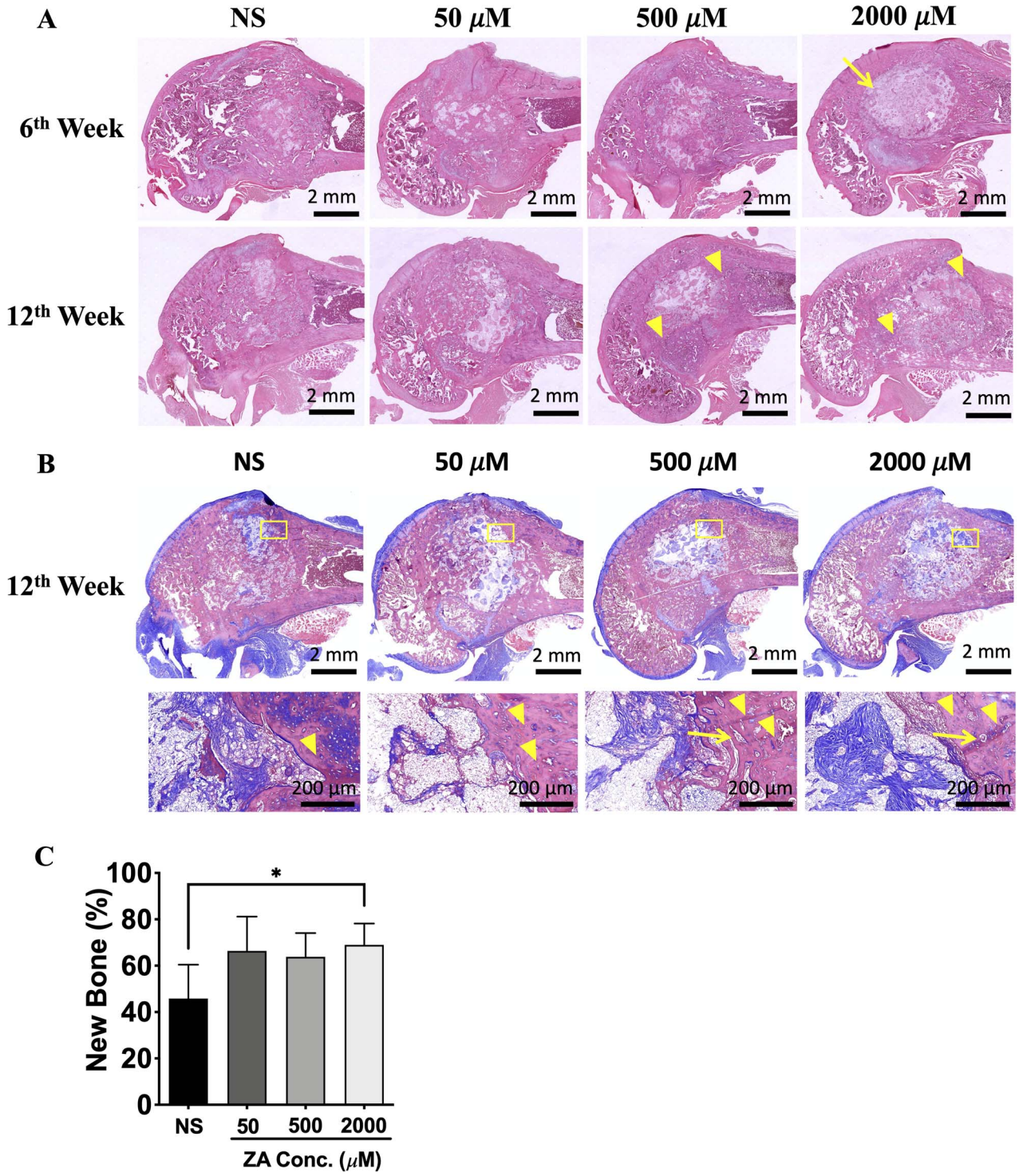

Figure 8. H&E staining (A). At the sixth week, significant bone resorption was observed in the NS group, and the implanted artificial bone was still visible in the 2000 μM group (A, yellow arrow). More deposition of osteoids surrounding the contact surface of scaffolds was observed in the 500 μM and 2000 μM groups but less in the NS group (A, yellow arrow head). Masson's trichrome staining revealed thick, dense bone-like tissue surrounding the implanted TCP scaffolds in the ZA-treated groups (B, yellow arrowhead). Neovascularization was evident inside the dense bone-like tissue (B, yellow arrow) in the 500 μM and 2000 μM group. Histomorphometric analysis (C) of the mineralized tissue area revealed a significantly higher value for the 2000 μM group than for the normal saline group (* $P < 0.05$).

with various concentrations of ZA. The results showed that a ZA concentration below 2.5×10^{-7} M did not have any adverse cytotoxic effects. Based on ALP and ARS staining and quantification of MC3T3-E1 cells and BMSCs, ZA did not have a negative impact on the osteoinductive ability of OIM. Additionally, the mRNA expression of ALP, OCN, and OPN in the ZA-treated groups was similar to that in the OIM only groups. A study using a polydopamine-coated porous titanium scaffold integrated with ZA-loaded gelatin nanoparticles demonstrated that extracts of the composite

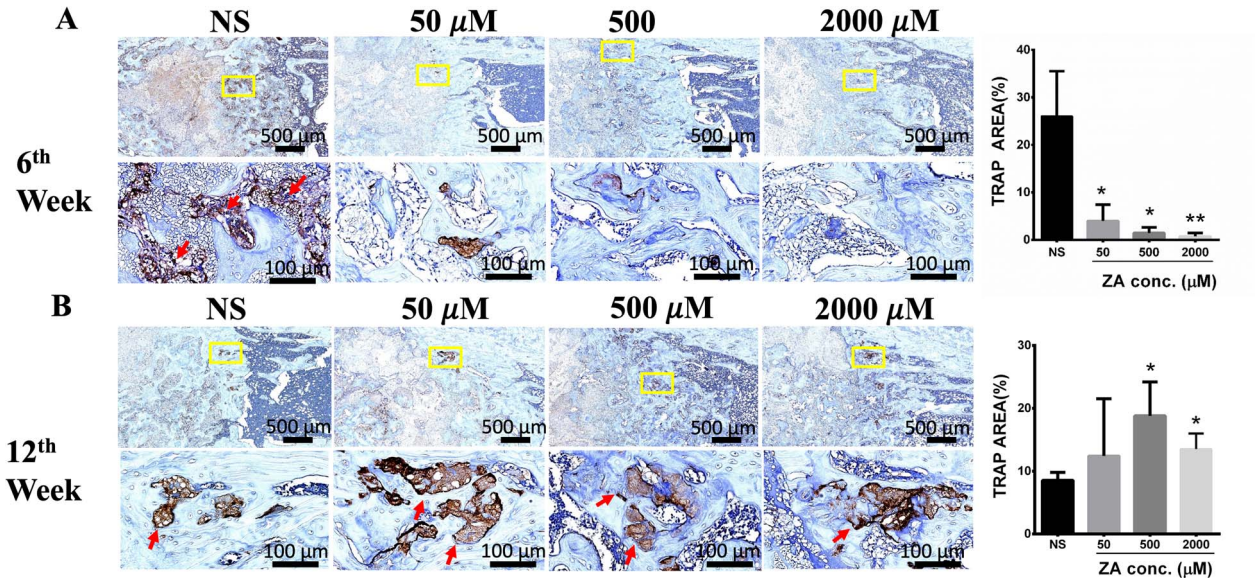

Figure 9. Immunohistochemistry with TRAP staining. In the sixth week, more TRAP-positive osteoclast cells were observed in the NS groups, and almost no cells with positive staining were present in the 500 μM and 2000 μM groups (a, red arrow). Quantification of the TRAP-staining revealed a significantly higher value for the normal saline groups than the ZA-treated groups (* $P < 0.05$, ** $P < 0.01$). More osteoclasts were found in the ZA-treated groups in the 12th week than in the 6th week (B, red arrow). Quantification of the TRAP-staining showed a significantly higher value for the 500 μM and 2000 μM groups than the normal saline groups (* $P < 0.05$).

scaffolds stimulated osteoblast differentiation and inhibited osteoclastogenesis at a ZA loading concentration of 50 μM.[13] Despite these positive findings, it was difficult to draw a convincing conclusion due to the uncontrolled ZA regimen, potential osteogenic effects of the scaffold, and uncontrolled ZA release in the repair of osteoporotic bone defects.[11,12,15] In this study, we used pure zolendronate (PHR1893, Sigma–Aldrich Corp., St. Louis, MO, USA) instead of a product from an intravenous regimen[11,43,44] to avoid potential effects from excipients. Several studies[45-48] have indicated that ZA, when administered at different doses and durations, can inhibit the osteogenesis of BMSCs, reduce the activity of osteoblasts, and ultimately hinder mineralization. Studies have shown that high doses of ZA can induce apoptosis in certain cell types, including osteoblasts, leading to reduced bone formation.[49,50] In our study, we ruled out the impact of cytotoxicity on osteogenic performance and concluded that ZA had no significant positive or negative effect on the osteogenic ability of BMSCs or preosteoblasts.

One study showed that ZA prevented the migration of osteoclast precursors and RANK expression during osteoclastogenesis through suppression of the NF-kB pathway, which was most likely related to changes in RANK expression.[51] Previous studies have indicated that ZA suppresses the non-canonical Wnt/Ca^{2+}/calmodulin-dependent protein kinase II pathway.[52,53] Some studies have also demonstrated that ZA is involved in the RANKL/RANK pathway.[32,39,53,54] Specifically, ZA modulates osteoclast apoptosis through activation of the NF-κB signaling pathway in an ovariectomized rat model.[55] Furthermore, ZA has been reported to inhibit the NF-κB pathway by promoting the deubiquitination of TRAF6.[56] Nonetheless, more research is still needed to elucidate the underlying mechanism. By using RANKL-induced RAW264.7 cells as a model, we examined the effects of ZA on osteoclastogenesis in the current work. In vitro TRAP staining and quantification showed that ZA suppressed osteoclast development if the dose was higher than 2.5×10^{-7} M. In the pit formation assay, even a lower dose of 10^{-9} M had a significant inhibitory effect on osteoclastogenesis. Furthermore, ZA inhibited osteoclastogenesis in part through the ERK and JNK pathways, as indicated by the inhibition of RANKL-induced expression of the Ctsk, NFATc1, TRAP, DC-STAMP, and c-Fos genes by ZA.[57,58]

Mitogen-activated protein kinases, or MAPKs, are a group of signaling molecules that play important roles in cellular processes such as proliferation, differentiation, and apoptosis.[30,39,41,53] There are several types of MAPKs, including c-Jun N-terminal kinase (JNK), p38, and extracellular signal-regulated kinase (ERK). In the context of osteoclast formation, previous studies have shown that MAPKs, particularly JNK and p38, promote the activation of c-Fos, a transcription factor that is essential for osteoclast differentiation.[25,39] Furthermore, MAPKs facilitate the translocation of activator protein-1 (AP-1), which is a transcription factor that regulates gene expression in response to a variety of stimuli, including cytokines and growth factors.[39,41] Inhibitors of ERK and JNK have been shown to block osteoclast differentiation in vitro and in vivo.[30,41,53,54] Studies showed ZA inhibited the RANKL-induced activation of NF-κB during osteoclastogenesis. However, the inhibitory mechanism of NF-κB by ZA on osteoclastogenesis is still controversial.[59,60] Our study showed that ZA significantly inhibited the phosphorylation of IκBα proteins within 5–15 min but had no significant effect on the phosphorylation of p65 proteins. The NF-κB family comprises five members with structural similarities, namely p50, p52, p65 (RelA), c-Rel, and RelB.[61,62] These proteins can homo- or heterodimerize, creating transcriptionally active NF-κB dimers. Typically, these dimers are kept inactive in the cytoplasm of quiescent cells by members of the inhibitory IκB protein family, which consists of at least seven proteins. The intricate regulatory mechanism between NF-κB and IκBα proteins could account for

the varied expression observed in our results for p65 and IκBα.

These inhibitors are being studied as potential therapeutic agents for conditions associated with excessive osteoclast activity, such as osteoporosis and bone metastasis. In our study, ZA inhibited the ERK and JNK signaling pathways, thus inhibiting the expression of the downstream factors c-Fos and NFATc1 and decreasing the expression of the fusion-related molecule DC-STAMP and the osteoclast-specific markers Ctsk and TRAP in RAW264.7 cells.

The purpose of the present study was to investigate the effect of ZA on early and late bone formation in a rat femoral critical-sized bone defect model when applied in combination with β-TCP artificial bone. The transformation of dosage from in vitro to in vivo local application typically encompasses intricate factors, such as the drug's pharmacokinetics and pharmacodynamics, the bioavailability of local application, and tissue characteristics.[63] In this research, distinguishing between radiographic and histological results at very low doses is challenging. The dosages utilized, reaching as high as 2000 μM, fall within a range where previous studies have indicated a clinically significant effect with local administration.[35] In a study where cancellous bone grafts were inserted into titanium chambers and implanted in the tibia of 50 male rats, it was observed that nearly the entire graft in all chambers had undergone revascularization but only partial remodeling at the 6-week harvest. The study concluded that local treatment led to denser bone and a reduced bone ingrowth distance compared to systemic treatment.[12] However, the mechanical impact of titanium chambers and local application via intravenous regimens cannot definitively attribute the bone formation solely to ZA. In another study, a polydopamine-coated porous titanium scaffold combined with ZA nanoparticles demonstrated enhanced biocompatibility and bone regeneration capability in 24 mature female rabbits.[13] However, the mechanisms underlying the sustained release of ZA for repairing osteoporotic bone defects at the molecular level and the pathway of dose-dependent anti-osteoclastogenesis remain unclear. It is important to note that confounding factors arising from both the titanium scaffold and nanoparticles prevent the definitive attribution of bone formation from ZA. In our investigation, we employed pure ZA without any artificial scaffold to eliminate potential influences from other confounding factors.

For the induction of new bone formation, regenerated osteoid, angiogenesis, and fibrosis are important evaluation parameters.[24,64] More osteoid formation, more neovascularization and less fibrotic tissue were observed after histological staining in the 500 μM and 2000 μM groups. More osteoclasts were found in the NS group in the sixth week, and sequential osteoclast formation was found in the ZA-treated groups, indicating that bone resorption was inhibited in the early callus formation stage without inhibition of late bone remodeling in the ZA-treated groups. The bone formation quantification results obtained from the Masson's trichrome histomorphometric data were compatible with the TRAP staining results from the 12th week.

After a single-dose intravenous administration, approximately half of the administered ZA will be eliminated from the body within 6 days due to its half-life of approximately 146 hours.[49,50,54] Despite its relatively brief half-life, ZA exhibits an extended duration of action owing to its strong binding to bone tissue.[17,18,54] Upon administration, the drug rapidly attaches to the host bone and is gradually released over a long period, resulting in a sustained impact on the bone tissue even after its rapid clearance from the bloodstream. In our in vivo study, ZA was incorporated into the bone graft rather than the host bone. As a result, in the sixth week, we observed a reduction in osteoclast formation in the surrounding bone graft. However, since ZA was absent in the new bone, we noted that the osteoclast activity return to normal in the 12th week compared to the sixth week. Based on our findings, the use of β-TCP artificial bone soaked with ZA at concentrations of 500 μM and 2000 μM appears to be a promising strategy for bone regeneration.

Our study has some limitations. First, the potential synergistic effect of ZA and β-TCP requires further clarification through longer soaking times and experimentation with different culture media. Second, for future applications, it would be worthwhile to investigate the efficacy of other bone graft substitutes, such as polymers, calcium sulfate, allografts and composite bone. Third, knockout animal models should be employed to confirm the pathways involved. Fourth, the use of a large animal model may help overcome individual differences arising from the ZA-sensitive dose-dependent effect. Finally, longer implantation periods and multiple time points are required to assess bone formation.

Conclusion

This study proved that local application of ZA maintains osteoblast viability while inhibiting the osteoclast activity, in part by suppressing the ERK and JNK signaling pathways. Our experiments showed that a β-TCP bone substitute soaked with ZA promotes new bone formation in rat femoral critical bone defects by impeding early osteoclast formation. Our results suggest that the local application of ZA in bone substitutes leads to increased osteoid formation in the final fused bone and may have potential for use in bone transplantation surgeries.

Acknowledgments

We would like to thank the Molecular Imaging Center, Expensive Advanced Instrument Core Laboratory and Microscopy Core Laboratory, Chang Gung Memorial Hospital, Linkou, Taiwan for their support in this project.

Author contributions

Ming-Kai Hsieh (Conceptualization, Investigation, Project administration, Writing – original draft), Chi-Yun Wang (Formal analysis, Resources, Software, Validation, Writing – review & editing), Fu-Cheng Kao (Conceptualization, Data curation, Writing – review & editing), Hui-Ting Su (Data curation, Formal analysis, Software, Validation, Visualization), Mei-Feng Chen (Methodology, Resources, Supervision, Validation), Tsung-Ting Tsai (Data curation, Investigation, Methodology, Supervision, Visualization), Po-Liang Lai (Conceptualization, Data curation, Supervision, Writing – review & editing).

Funding

This work was supported by Chang Gung Memorial Hospital, Taiwan (grant nosCMRPG3M0371; CMRPG3M0372).

Conflicts of interest

None.

Data availability

The data that support the findings of this study are available from the corresponding author, Po-Liang Lai, upon reasonable request.

References

1. Pereira HF, Cengiz IF, Silva FS, Reis RL, Oliveira JM. Scaffolds and coatings for bone regeneration. *J Mater Sci Mater Med*. 2020;31(3):27, 1–16. https://doi.org/10.1007/s10856-020-06364-y.
2. Shibuya N, Jupiter DC. Bone graft substitute: allograft and xenograft. *Clin Podiatr Med Surg*. 2015;32(1):21–34. https://doi.org/10.1016/j.cpm.2014.09.011.
3. Kim DM, Hong H, Lin JC-Y, Nevins M. Evaluation of the bone-regenerating effects of two Anorganic bovine bone grafts in a critical-sized alveolar ridge defect model. *Int J Periodontics Restorative Dent*. 2017;37(4):e234–e244. https://doi.org/10.11607/prd.3305.
4. Lissenberg-Thunnissen SN, DeGorter DJJ, Sier CFM, Schipper IB. Use and efficacy of bone morphogenetic proteins in fracture healing. *Int Orthop*. 2011;35(9):1271–1280. https://doi.org/10.1007/s00264-011-1301-z.
5. Wu CC, Huang YK, Chang WJ, Wu YC, Wang CC, Yang KC. Limitation of the antibiotic-eluting bone graft substitute: an example of gentamycin-impregnated calcium sulfate. *J Biomed Mater Res - Part B Appl Biomater*. 2018;106(1):80–87. https://doi.org/10.1002/jbm.b.33815.
6. Wang W, Yeung KWK. Bone grafts and biomaterials substitutes for bone defect repair: a review. *Bioact Mater*. 2017;2(4):224–247. https://doi.org/10.1016/j.bioactmat.2017.05.007.
7. Rao M, Awasthi M. A review on interventions to prevent osteoporosis and improve fracture healing in osteoporotic patients. *AIMS Med Sci*. 2020;7(4):243–268. https://doi.org/10.3934/MEDSCI.2020015.
8. Sølling AS, Harsløf T, Langdahl B. Treatment with zoledronate subsequent to denosumab in osteoporosis: a randomized trial. *J Bone Miner Res*. 2020;35(10):1858–1870. https://doi.org/10.1002/JBMR.4098.
9. Black DM, Delmas PD, Eastell R, et al. Once-yearly zoledronic acid for treatment of postmenopausal osteoporosis. *N Engl J Med*. 2007;356(18):1809–1822. https://doi.org/10.1056/NEJMOA067312.
10. Zhou J, Ma X, Wang T, Zhai S. Comparative efficacy of bisphosphonates in short-term fracture prevention for primary osteoporosis: a systematic review with network meta-analyses. *Osteoporos Int*. 2016;27:3289–3300. https://doi.org/10.1007/s00198-016-3654-z.
11. Belfrage O, Isaksson H, Tägil M. Local treatment of a bone graft by soaking in zoledronic acid inhibits bone resorption and bone formation. A bone chamber study in rats. *BMC Musculoskelet Disord*. 2012;13:240, 1–8. https://doi.org/10.1186/1471-2474-13-240,1.
12. Belfrage O, Flivik G, Sundberg M, Kesteris U, Tägil M. Local treatment of cancellous bone grafts with BMP-7 and zoledronate increases both the bone formation rate and bone density: a bone chamber study in rats. *Acta Orthop*. 2011;82(2):228–233. https://doi.org/10.3109/17453674.2011.566138.
13. Yang X-J, Wang FQ, Lu CB, et al. Modulation of bone formation and resorption using a novel zoledronic acid loaded gelatin nanoparticles integrated porous titanium scaffold: an in vitro and in vivo study. *Biomed Mater*. 2020;15:055013. https://doi.org/10.1088/1748-605X/ab8720,5.
14. Manabe T, Mori S, Mashiba T, et al. Effect of dosing interval duration of intermittent ibandronate treatment on the healing process of femoral osteotomy in a rat fracture model. *Calcif Tissue Int*. 2012;90(3):193–201. https://doi.org/10.1007/s00223-011-9563-4.
15. Sharma D, Hamlet SM, Petcu EB, Ivanovski S. The effect of bisphosphonates on the endothelial differentiation of mesenchymal stem cells. *Sci Reports*. 2016;6(1):1–11. https://doi.org/10.1038/srep20580.
16. von Knoch F, Jaquiery C, Kowalsky M, et al. Effects of bisphosphonates on proliferation and osteoblast differentiation of human bone marrow stromal cells. *Biomaterials*. 2005;26(34):6941–6949. https://doi.org/10.1016/j.biomaterials.2005.04.059.
17. Chen B, Li Y, Yang X, Xu H, Xie D. Zoledronic acid enhances bone-implant osseointegration more than alendronate and strontium ranelate in ovariectomized rats. *Osteoporos Int*. 2013;24(7):2115–2121. https://doi.org/10.1007/s00198-013-2288-7.
18. Mavi E, Hocaoglu PT. Effects of a single intravaneous dose of zoledronic acid on bone healing following tooth extraction in ovariectomized rabbits. *Saudi Dent J*. 2021;33(7):724–730. https://doi.org/10.1016/J.SDENTJ.2020.03.016.
19. Dikicier E, Karaçayli Ü, Dikicier S, Günaydin Y. Effect of systemic administered zoledronic acid on osseointegration of a titanium implant in ovariectomized rats. *J Cranio-Maxillofacial Surg*. 2014;42(7):1106–1111. https://doi.org/10.1016/j.jcms.2014.01.039.
20. Hsieh MK, Wu CJ, Chen CC, et al. BMP-2 gene transfection of bone marrow stromal cells to induce osteoblastic differentiation in a rat calvarial defect model. *Mater Sci Eng C*. 2018;91:806–816. https://doi.org/10.1016/j.msec.2018.06.004.
21. Hsieh MK, Khai-Woon Toh E, Tsai TT, Niu CC, Wu SC, Lai PL. Plasmid BMP-2–embedded gelatin sponge as a gene-activated matrix for preosteoblast differentiation. *J Drug Deliv Sci Technol*. 2019;53:101129, 1–7. https://doi.org/10.1016/j.jddst.2019.101129.
22. Mei G, Zou Z, Fu S, et al. Substance P activates the Wnt signal transduction pathway and enhances the differentiation of mouse Preosteoblastic MC3T3-E1 cells. *Int J Mol Sci*. 2014;15(4):6224. https://doi.org/10.3390/IJMS15046224,6240.
23. Lucy TT, Mamun-Or-rashid ANM, Yagi M, Yonei Y. Serial passaging of RAW 264.7 cells modulates intracellular AGE formation and downregulates RANKL-induced in vitro osteoclastogenesis. *Int J Mol Sci*. 2022;23(4):1–19. https://doi.org/10.3390/IJMS23042371.
24. Hsieh MK, Wu CJ, Su XC, et al. Bone regeneration in ds-red pig calvarial defect using allogenic transplantation of EGFP-pMSCs – a comparison of host cells and seeding cells in the scaffold. *PLoS One*. 2019;14(7):e0215499. https://doi.org/10.1371/journal.pone.0215499.
25. Tokunaga T, Mokuda S, Kohno H, et al. TGFβ1 regulates human RANKL-induced osteoclastogenesis via suppression of NFATc1 expression. *Int J Mol Sci*. 2020;21(3):800. https://doi.org/10.3390/IJMS21030800.
26. Wang C-Y, Kuo ZK, Hsieh MK, et al. Cell migration of preosteoblast cells on a clinical gelatin sponge for 3D bone tissue engineering. *Biomed Mater*. 2019;15(1):015005. https://doi.org/10.1088/1748-605x/ab4fb5.
27. Yu NYC et al. In vivo local co-delivery of recombinant human bone morphogenetic protein-7 and pamidronate via poly-D, L-lactic acid. *Eur Cell Mater*. 2010;20:431–442. https://doi.org/10.22203/ECM.V020A35.
28. Zhou Y, Mohan A, Moore DC, et al. SHP2 regulates osteoclastogenesis by promoting preosteoclast fusion. *FASEB J*. 2015;29(5):1635–1645. https://doi.org/10.1096/fj.14-260844.
29. Vesprey A, Yang W. Pit assay to measure the bone resorptive activity of bone marrow-derived osteoclasts. *Bio-protocol*. 2016;6(12):1–10. https://doi.org/10.21769/BIOPROTOC.1836.
30. Li L, Sapkota M, Gao M, Choi H, Soh Y. Macrolactin F inhibits RANKL-mediated osteoclastogenesis by suppressing Akt, MAPK and NFATc1 pathways and promotes osteoblastogenesis through a BMP-2/smad/Akt/Runx2 signaling pathway. *Eur J Pharmacol*. 2017;815:202–209. https://doi.org/10.1016/j.ejphar.2017.09.015.
31. Elson A, Anuj A, Barnea-Zohar M, Reuven N. The origins and formation of bone-resorbing osteoclasts. *Bone*. 2022;164:116538. https://doi.org/10.1016/j.bone.2022.116538.

32. Jeong DH, Kwak SC, Lee MS, Yoon KH, Kim JY, Lee CH. Betulinic acid inhibits RANKL-induced osteoclastogenesis via attenuating Akt, NF-κB, and PLCγ2-Ca2+ signaling and prevents inflammatory bone loss. *J Nat Prod*. 2020;83(4):1174–1182. https://doi.org/10.1021/ACS.JNATPROD.9B01212.
33. Kim JM, Yang YS, Park KH, Oh H, Greenblatt MB, Shim JH. The ERK MAPK pathway is essential for skeletal development and homeostasis. *Int J Mol Sci*. 2019;20(8):1–14. https://doi.org/10.3390/ijms20081803.
34. Munshi A, Ramesh R. Mitogen-activated protein kinases and their role in radiation response. *Genes and Cancer*. 2013;4(9–10):401–408. https://doi.org/10.1177/1947601913485414.
35. Jakobsen T, Baas J, Bechtold JE, Elmengaard B, Søballe K. The effect of soaking allograft in bisphosphonate: a pilot dose-response study. *Clin Orthop Relat Res*. 2010;468(3):867–874. https://doi.org/10.1007/S11999-009-1099-9.
36. Strickland A, Cavanaugh D, Leatherwood WH, Raynor J, Brown A, Weinhold PS. Effect of local zoledronic acid administration in a rat model of posterolateral spinal fusion. *J Orthop*. 2019;17:101–105. https://doi.org/10.1016/J.JOR.2019.08.021.
37. Liu Z, Yu Z, Chang H, et al. Strontium-containing α-calcium sulfate hemihydrate promotes bone repair via the TGF-β/Smad signaling pathway. *Mol Med Rep*. 2019;20(4):3555–3564. https://doi.org/10.3892/mmr.2019.10592.
38. Chen Y-C, Hsu P-Y, Tuan W, Lai P-L. From phase diagram to the design of strontium-containing carrier. *J Asian Ceram Soc*. 2020;8(3):677–684. https://doi.org/10.1080/21870764.2020.1774972.
39. Li DZ, Zhang QX, Dong XX, Li HD, Ma X. Treatment with hydrogen molecules prevents RANKL-induced osteoclast differentiation associated with inhibition of ROS formation and inactivation of MAPK, AKT and NF-kappa B pathways in murine RAW264.7 cells. *J Bone Miner Metab*. 2014;32(5):494–504. https://doi.org/10.1007/S00774-013-0530-1.
40. Cao J, Zhou MX, Chen X, et al. Sec-O-Glucosylhamaudol inhibits RANKL-induced osteoclastogenesis by repressing 5-LO and AKT/GSK3β signaling. *Front Immunol*. 2022;13:1–12. https://doi.org/10.3389/fimmu.2022.880988.
41. Lee K, Chung YH, Ahn H, Kim H, Rho J, Jeong D. Selective regulation of MAPK signaling mediates RANKL-dependent osteoclast differentiation. *Int J Biol Sci*. 2016;12(2):235. https://doi.org/10.7150/IJBS.13814,245.
42. Datta HK, Vila J, Tuck SP. Long-term evaluation of anabolic and anti-resorptive agents in adults with familial osteoporosis due to pro205ala variant of the col1a1 gene. *Osteoporos Int*. 2021;32(10):2105–2109. https://doi.org/10.1007/S00198-021-05933-3.
43. Gao Y, Luo E, Hu J, Xue J, Zhu S, Li J. Effect of combined local treatment with zoledronic acid and basic fibroblast growth factor on implant fixation in ovariectomized rats. *Bone*. 2009;44(2):225–232. https://doi.org/10.1016/J.BONE.2008.10.054.
44. Salzano G, Marra M, Porru M, et al. Self-assembly nanoparticles for the delivery of bisphosphonates into tumors. *Int J Pharm*. 2011;403(1–2):292–297. https://doi.org/10.1016/j.ijpharm.2010.10.046.
45. Thibaut F, Watrin T, Meary F, et al. Effects of zoledronic acid on osteoblasts in three-dimensional culture. *J Dent Sci*. 2015;10(1):8–15. https://doi.org/10.1016/J.JDS.2014.07.004.
46. Orriss IR, Key ML, Colston KW, Arnett TR. Inhibition of osteoblast function in vitro by aminobisphosphonates. *J Cell Biochem*. 2009;106(1):109–118. https://doi.org/10.1002/JCB.21983.
47. Maruotti N, Corrado A, Neve A, Cantatore FP. Bisphosphonates: effects on osteoblast. *Eur J Clin Pharmacol*. 2012;68(7):1013–1018. https://doi.org/10.1007/S00228-012-1216-7.
48. Basso FG, Paula A, Turrioni S, Hebling J, DeSouza Costa CA. "E-mail experimental section / original paper zoledronic acid inhibits human osteoblast activities," *Gerontology*. 2013;59(6):534–541. https://doi.org/10.1159/000351194.
49. Huang X, Huang S, Guo F, et al. Dose-dependent inhibitory effects of zoledronic acid on osteoblast viability and function in vitro. *Mol Med Rep*. 2016;13(1):613–622. https://doi.org/10.3892/MMR.2015.4627.
50. Wang L, Liu Y, Zhou Y, et al. Zoledronic acid inhibits the growth of cancer stem cell derived from cervical cancer cell by attenuating their stemness phenotype and inducing apoptosis and cell cycle arrest through the Erk1/2 and Akt pathways. *J Exp Clin Cancer Res*. 2019;38(1):1–18. https://doi.org/10.1186/S13046-019-1109-Z,93.
51. Kimachi K, Kajiya H, Nakayama S, Ikebe T, Okabe K. Zoledronic acid inhibits RANK expression and migration of osteoclast precursors during osteoclastogenesis. *Naunyn Schmiedeberg's Arch Pharmacol*. 2011;383(3):297–308. https://doi.org/10.1007/s00210-010-0596-4.
52. Sadr-Eshkevari P, Ashnagar S, Rashad A, et al. Bisphosphonates and connexin 43: a critical review of evidence. *Cell Commun Adhes*. 2014;21(5):241–247. https://doi.org/10.3109/15419061.2014.927869.
53. Boudot C, Saidak Z, Boulanouar AK, et al. Implication of the calcium sensing receptor and the phosphoinositide 3-kinase/Akt pathway in the extracellular calcium-mediated migration of RAW 264.7 osteoclast precursor cells. *Bone*. 2010;46(5):1416–1423. https://doi.org/10.1016/j.bone.2010.01.383.
54. Wang L, Fang D, Xu J, Luo R. Various pathways of zoledronic acid against osteoclasts and bone cancer metastasis: a brief review. *BMC Cancer*. 2020;20(1):1059. https://doi.org/10.1186/S12885-020-07568-9.
55. Cheng YT, Liao J, Zhou Q, et al. Zoledronic acid modulates osteoclast apoptosis through activation of the NF-κB signaling pathway in ovariectomized rats. *Exp Biol Med*. 2021;246(15):1727–1739. https://doi.org/10.1177/15353702211011052.
56. Huang XL, Huang LY, Cheng YT, et al. Zoledronic acid inhibits osteoclast differentiation and function through the regulation of NF-κB and JNK signalling pathways. *Int J Mol Med*. 2019;44(2):582–592. https://doi.org/10.3892/ijmm.2019.4207.
57. Wada T, Nakashima T, Hiroshi N, Penninger JM. RANKL-RANK signaling in osteoclastogenesis and bone disease. *Trends Mol Med*. 2006;12(1):17–25. https://doi.org/10.1016/J.MOLMED.2005.11.007.
58. Lee K, Seo I, Choi H, Jeong D. Molecular sciences roles of mitogen-activated protein kinases in osteoclast biology. *Int J Mol Sci*. 2018;19(10):3004, 1–20. https://doi.org/10.3390/ijms19103004.
59. Khosla S, Shane E. A crisis in the treatment of osteoporosis. *J Bone Miner Res*. 2016;31(8):1485–1487. https://doi.org/10.1002/JBMR.2888.
60. Nakagawa T, Ohta K, Uetsuki R, et al. Zoledronate inhibits osteoclast differentiation via suppressing vascular endothelial growth factor receptor 2 expression. *Biochem Genet*. 2020;58(3):473–489. https://doi.org/10.1007/S10528-020-09961-2.
61. Hayden MS, Ghosh S. Shared principles in NF-kappaB signaling. *Cell*. 2008;132(3):344–362. https://doi.org/10.1016/J.CELL.2008.01.020.
62. Gilmore TD. Introduction to NF-kappaB: players, pathways, perspectives. *Oncogene*. 2006;25(51):6680–6684. https://doi.org/10.1038/SJ.ONC.1209954.
63. Veloso C, Videira RA, Andrade PB, Cardoso C, Vitorino C. Topical fixed-dose combinations: current in vitro methodologies for preclinical development. *Int J Pharm*. 2022;617:121621, 1–11. https://doi.org/10.1016/J.IJPHARM.2022.121621.
64. Kargozar S, Mozafari M, Hashemian SJ, et al. Osteogenic potential of stem cells-seeded bioactive nanocomposite scaffolds: a comparative study between human mesenchymal stem cells derived from bone, umbilical cord Wharton's jelly, and adipose tissue. *J Biomed Mater Res - Part B Appl Biomater*. 2018;106(1):61–72. https://doi.org/10.1002/jbm.b.33814.